Title

Genetic mutations in Ca2+ signaling alter dendrite morphology and social approach in juvenile mice

Journal

Genes Brain & Behavior, 18(1)

ISSN

1601-1848

Authors

Keil, Kimberly P

Sethi, Sunjay

Wilson, Machelle D

et al.

Publication Date

2019

DOI

10.1111/gbb.12526

Peer reviewed

Received: 31 July 2018 | Revised: 5 October 2018 | Accepted: 9 October 2018

DOI: 10.1111/gbb.12526

Genes, Brain and Behavior

ORIGINAL ARTICLE

Genetic mutations in Ca^{2+} signaling alter dendrite morphology and social approach in juvenile mice

Kimberly P. Keil[1] | Sunjay Sethi[1] | Machelle D. Wilson[2] | Jill L. Silverman[3,4] | Isaac N. Pessah[1,4] | Pamela J. Lein[1,4]

[1]Department of Molecular Biosciences, University of California-Davis, School of Veterinary Medicine, Davis, California

[2]Clinical and Translational Science Center, Department of Public Health Sciences, Division of Biostatistics, University of California-Davis, School of Medicine, Davis, California

[3]Department of Psychiatry and Behavioral Sciences, University of California-Davis School of Medicine, Sacramento, California

[4]MIND Institute, University of California-Davis, School of Medicine, Sacramento, California

Correspondence
Pamela J. Lein, Department of Molecular Biosciences, School of Veterinary Medicine, University of California, Davis. 1089 Veterinary Medicine Drive, Davis, CA 95616.
Email: pjlein@ucdavis.edu

Funding information
Eunice Kennedy Shriver National Institute of Child Health and Human Development, Grant/Award Number: HD079125HD088016; Floyd and Mary Schwall Medical Research Fellowship Program, Grant/Award Number: Predoctoral Fellowship; National Center for Advancing Translational Sciences, Grant/Award Number: TR000002; National Institute of Environmental Health Sciences, Grant/Award Number: ES007059ES011269ES014901; U.S. Environmental Protection Agency, Grant/Award Number: R833292

Dendritic morphology is a critical determinant of neuronal connectivity, and calcium signaling plays a predominant role in shaping dendrites. Altered dendritic morphology and genetic mutations in calcium signaling are both associated with neurodevelopmental disorders (NDDs). In this study we tested the hypothesis that dendritic arborization and NDD-relevant behavioral phenotypes are altered by human mutations that modulate calcium-dependent signaling pathways implicated in NDDs. The dendritic morphology of pyramidal neurons in CA1 hippocampus and somatosensory cortex was quantified in Golgi-stained brain sections from juvenile mice of both sexes expressing either a human gain-of-function mutation in ryanodine receptor 1 (T4826I-*RYR1*), a human CGG repeat expansion (170-200 CGG repeats) in the fragile X mental retardation gene 1 (*FMR1* premutation), both mutations (double mutation; DM), or wildtype mice. In hippocampal neurons, increased dendritic arborization was observed in male T4826I-*RYR1* and, to a lesser extent, male *FMR1* premutation neurons. Dendritic morphology of cortical neurons was altered in both sexes of *FMR1* premutation and DM animals with the most pronounced differences seen in DM females. Genotype also impaired behavior, as assessed using the three-chambered social approach test. The most striking lack of sociability was observed in DM male and female mice. In conclusion, mutations that alter the fidelity of calcium signaling enhance dendritic arborization in a brain region- and sex-specific manner and impair social behavior in juvenile mice. The phenotypic outcomes of these mutations likely provide a susceptible biological substrate for additional environmental stressors that converge on calcium signaling to determine individual NDD risk.

KEYWORDS

autism, developmental neurobiology, FMR1, Golgi stain Sholl analysis, ryanodine receptor

1 | INTRODUCTION

Neurodevelopmental disorders (NDDs), including intellectual disability, attention deficit hyperactivity disorder, and autism spectrum disorders, impart a significant healthcare and quality of life burden to patients and their families.[1,2] Such data provide a compelling reason to identify and characterize risk factors that confer NDD susceptibility. Although no single genetic component can account for most NDDs,[3–5] it has long been acknowledged that the genetic background of an individual can influence risk.[6–8] A significant number of genes implicated in NDDs encode proteins that either function to generate calcium (Ca^{2+}) signals or are regulated by Ca^{2+}.[9–11] Ca^{2+}-dependent signaling pathways are largely responsible for driving the dynamic structural remodeling of dendrites that occurs during development.[12–15] Because dendritic architecture is a critical determinant of neural networks, and altered dendritic morphology (increased or decreased dendrite number, branching, spine density, etc.) is associated with many NDDs,[11,16–20] these observations suggest mutations

that alter the fidelity of Ca^{2+} signaling influence NDD risk, in part, by interfering with dendritic arborization in the developing brain.

To test this hypothesis, we quantified dendritic morphology and social behavior in juvenile mice expressing human mutations known to alter Ca^{2+} signaling in neurons. One such mutation is T4826I-*RYR1*, a human gain-of-function mutation in the gene that encodes ryanodine receptor 1 (RyR1), an essential regulator of intracellular calcium stores.[21,22] It is estimated that ~35% of the human population carry one or more *RYR1* genetic variant.[23] Gain-of-function mutations in the human *RYR1* gene underlie malignant hyperthermia susceptibility (MHS), which predisposes carriers to acute, potentially lethal, hyperthermia in response to heat stress, anesthetics, and other environmental stressors.[10,24] RyR activity is necessary for BDNF-induced remodeling of dendritic spines,[25] and RyR1 activity is required for activity-dependent dendritic growth and synaptogenesis.[26,27] These observations suggest the possibility that gain-of-function *RYR1* mutations alter dendritic arborization in the developing brain.

A second human mutation known to alter neuronal Ca^{2+} signaling is the CGG expansion repeat mutation in fragile X mental retardation gene 1 (*FMR1*).[28–31] CGG repeat expansions in the 5′ non-coding region of *FMR1* in the premutation range (55-200 CGG repeats) not only give rise to the neurodegenerative disorder fragile X-associated tremor/ataxia syndrome (FXTAS), but also increase risk for NDDs.[32–35] Estimated prevalence of the *FMR1* premutation is 1:209 in females and 1:430 in males.[36] A knock-in mouse that expresses the human *FMR1* premutation (170-200 CGG repeats) exhibits pathology consistent with human carriers or FXTAS patients, including increased *FMR1* mRNA, decreased FMRP, ubiquitin-positive intranuclear inclusions and deficits in spatial learning and memory and motor behavior in adult animals.[31,37–39] The *FMR1* premutation mouse has also been reported to exhibit aberrant neural migration,[40] and primary neurons derived from *FMR1* premutation mice have significantly altered dendritic arborization,[41] increased resting intracellular Ca^{2+} concentrations, abnormal patterns of spontaneous Ca^{2+} oscillations and altered responses to glutamate in central neurons and astrocytes.[29,30] Several early deficits identified in the premutation mouse model have been corroborated in human iPSC-derived neurons from FMR1 premutation patients.[42]

In the present study, we quantified dendritic arborization and social approach behavior in both the T4826I-*RYR1* and *FMR1* premutation mouse models. Because many NDDs, such as autism, have a complex etiology and are thought to arise from multiple genetic hits, and because dysregulated calcium signaling is observed in NDDs,[9–11] we also tested the hypothesis that expression of two mutations that alter calcium signaling amplifies the effect of either mutation expressed singly. To test this, we crossed homozygous T4826I-*RYR1* MHS (T4826I mice) with homozygous female or hemizygous male *FMR1* premutation mice (CGG mice) to generate double mutant (DM) homozygous/homozygous female or homozygous/hemizygous male mice. Our findings indicate that genetic mutations that alter Ca^{2+} signaling interfere with dendritic architecture in pyramidal neurons in the CA1 hippocampus and adjacent somatosensory cortex of juvenile mice in a sex specific manner. These mutations also disrupt social behavior in juvenile mice.

2 | METHODS

2.1 | Animals

All procedures involving animals were conducted in accordance with the NIH Guide for the Care and Use of Laboratory Animals and were approved by the University of California-Davis Animal Care and Use Committee. Male and female mice of four different genotypes were investigated: (a) homozygous T4826I-*RYR1* mice, which express a human gain-of-function mutation in *RYR1* referred to as T4826I mice[21,22]; (b) female homozygous and male hemizygous *FMR1* premutation mice that express the X-linked CGG repeat expansion mutation in the *FMR1* gene with the number of X-linked CGG repeats in the premutation range ranging from 170 to 200, referred to as CGG mice[29,31]; (c) mice expressing both the T4826I (homozygous males and homozygous females) and CGG (hemizygous males; homozygous females) mutations, referred to as double mutation (DM) mice; and (d) wildtype (WT) mice (75% C57BL/6J/25% SVJ129 genetic background). C57BL/6J and SVJ129 WT mice were purchased from Jackson Labs (Sacramento, CA) and crossed to generate the 75% C57BL/6J / 25% SVJ129 genetic background of the WT mice, which was determined by SNP analysis to match the genetic background of the mutant genotypes. The following female x male matings were used to generate the juvenile mice that were tested at postnatal day (P) 25-30: Homozygous x homozygous T4826I, homozygous x hemizygous CGG, homozygous T4826I / homozygous CGG x homozygous T4826I / hemizygous CGG to generate DM mice, and WT x WT (WT). All mice were housed in clear plastic shoebox cages containing corn cob bedding and maintained on a 12 hours light and dark cycle at 22 ± 2°C. Feed (Diet 5058, LabDiet, Saint Louis, Missouri) and water were available ad libitum. After weaning at P21, animals were group housed with same genotype, same sex littermates prior to behavioral testing, which has been reported to not alter social approach behavior.[43]

2.2 | Genotyping

DNA was extracted from ear punches obtained from P21 mice by incubating tissue in 25 μL of digestion buffer (50 mM TRIS, 1 nM EDTA, 25 mM NaCl, 0.25% SDS, pH 8, Sigma, Saint Louis, Missouri) and 0.5 μL of Proteinase K (20 mg/mL, Amresco-VWR, Radnor, Pennsylvania) overnight at 56°C. Samples were diluted with 250 μL of ultrapure water and heated to 100°C for 5 minutes. CGG repeat lengths were determined using Expanded High Fidelity Plus PCR System (Roche Diagnostics, Indianapolis, Indiana) as described previously.[41] Genotyping of T4826I was conducted using previously described WT and T4826I mutant primer sequences[21] under the following PCR conditions: (a) for T4826I mutant *RYR1*: a final concentration of 0.5 μM each of forward and reverse primers, 1x GoTaq buffer, 2 mM MgCl2, 0.4 mM dNTP and 0.25 μL GoTaq Polymerase (Promega, Madison, Wisconsin) to a final volume of 25 μL; and (b) for the WT *RYR1*: a final concentration of 0.53 μM forward primer, 0.57 μM reverse primer, 1x GoTaq buffer, 2 mM MgCl2, 0.4 mM dNTP, and 0.25 μL GoTaq Polymerase to a final volume of 25 μL. PCR conditions were as follows: (a) for T4826I mutant *RYR1*: 95°C for 3 minutes, 40 cycles of 95°C for 30 seconds, 60°C for 30 seconds,

72°C for 30 seconds and a final extension of 72°C for 10 minutes; and (b) for the WT *RYR1*: same as above except annealing step occurs at 55°C for 30 seconds. PCR products were separated on a 1.5% agarose gel at 125 V for 30 minutes; expected size of the T4826I mutant *RYR1* band was 100 bp; the WT *RYR1* band, 353 bp.

2.3 | Social approach

The three-chambered social approach was conducted as described previously.[44–47] Animals were moved to the room 1 hour prior to testing. Testing was conducted during the light phase. Light level in the room was 110 lx. Testing consisted of three consecutive 10 minutes phases. During the first phase, animals were placed in the center of a three-chambered box for 10 minutes to acclimate. During the second, habituation phase, the center divide doors were removed and animals were allowed to explore the entire box for 10 minutes. During the third 10-minute phase, animals were allowed to interact with either an empty cup (object) or a cup with a novel age- and sex-matched WT mouse placed on opposite sides of the center chamber. Placement of the object and mouse on left or right sides of the chamber was counterbalanced to eliminate side bias. Chamber and cups were cleaned with 70% ethanol between each animal. If an animal failed to explore they were removed from the study. Animals used as novel mice were habituated to sitting under the wire cup for 10 minutes. Behavior was analyzed using Noldus EthoVision XT (version 11.0) automated tracking and analysis software (Noldus Information Technology Inc., Leesburg, Virginia). Male/Female n = 11/15 WT, 10/10 T4826I, 9/11 CGG, 13/11 DM animals each from at least 6 independent litters.

2.4 | Golgi staining

Golgi staining was performed using the FD Rapid GolgiStain kit (FD NeuroTechnologies Inc. Columbia, Maryland) according to manufacturer's instructions as described previously.[48,49] Brightfield images of Golgi-stained neurons (n = 32-48 neurons per sex per genotype from at least six independent mice) were acquired with an IX-81 inverted microscope (Olympus, Shinjuku, Japan) using MetaMorph Image Analysis Software (version 7.1, Molecular Devices, Sunnyvale, California). Neurons were acquired from CA1 dorsal hippocampus and somatosensory cortex in slices ranging from ~ −2.3 to −1.4 mm Bregma. Criteria for selection of neurons were as described previously.[48,50] Basilar dendritic arbors of neurons were traced by an individual blinded to experimental group using NeuroLucida (version 11, MBF Bioscience, Williston, Vermont), and arbor complexity was quantified by automated branch structure and Sholl analysis using NeuroLucida Explorer (version 11, MBF Bioscience). Figure S1 illustrates the endpoints examined in Golgi-stained neurons. Neuron tracings are publicly available via the NeuroMorpho.Org database (NeuroMorpho.Org).

2.5 | Statistics

Golgi-stained neurons from juvenile brain sections were analyzed using a mixed effects model as previously described.[48,49] All analyses were conducted using SAS software (version 9.4) of the SAS System for Windows (SAS Institute Inc., Cary, North Carolina). For multi-level data, if an outcome variable did not appear to be normal based on histograms, summary statistics and residual plots, or if unequal variances were observed, the appropriate transformation was used to achieve approximate normality, and Satterthwaite degrees of freedom were used in the mixed model to account for unequal variance. Area under the curve for the number of dendritic intersections, values for the distance from the soma of the peak number of dendritic intersections (peak X), and the maximum number of dendritic intersections (peak Y) were calculated from Sholl profiles using built in area under the curve analysis in GraphPad Prism Software (v6.07, San Diego, California). Table S1 summarizes least squares means data, including group estimates and SE. Differences in least squares means were used to determine significant differences within a sex or between sexes of each genotype, and data from all groups are summarized in Table S2 (including estimate, SE, degrees of freedom, t value and P value). For all other endpoints, data were assessed for normality and homogeneity of variance using the Shapiro-Wilks test and F test respectively using GraphPad Prism. Differences between two groups were assessed using Student's t test or Student's t test with Welch's correction for parametric data and by the Mann Whitney U test for nonparametric data. Differences between more than two groups were assessed using one-way ANOVA followed by Newman-Keuls multiple comparison test for parametric data or Kruskal-Wallis test followed by Dunn's multiple comparison test for nonparametric data. Data are reported as mean ± SE for Sholl plots, and box and whisker plots indicate the mean as a (+) and whiskers are 10-90th percentile, P values ≤0.05 were considered significant.

3 | RESULTS

3.1 | Dendritic morphology varies between sexes and genotypes

Results from the mixed effects statistical modeling used to examine the effects of sex, genotype, and sex*genotype interactions on specific parameters of dendritic morphology variable are summarized in Table 1. For ease of interpretation, we first discuss sex, genotype or sex*genotype interactions that were identified, and then discuss differences within sex or genotype, summarized in Table 2; Table S2. Data collected from pyramidal CA1 hippocampal neurons are presented first, followed by data from pyramidal neurons of the somatosensory cortex. These brain regions were chosen because both have been implicated in NDDs, such as autism. Changes in connectivity have been reported in the hippocampus[51] and the somatosensory cortex of patients with autism vs neurotypical controls.[52,53] Changes in hippocampal volume,[54–56] and reduced branching of CA1 hippocampal neurons have also been reported in brains of autism vs neurotypical controls.[57] Furthermore, changes in neural organization and density in the hippocampus have been correlated with social deficits in a rat model of autism.[58] These brain regions also serve as anatomic substrates of social behavior in humans[59,60] and preclinical models.[61–63]

Sholl plots and representative images of the basilar dendritic arbor of Golgi-stained pyramidal CA1 hippocampal neurons for each sex and genotype are shown in Figure 1A-C. Genotype differences

TABLE 1 Differences in dendrite morphology of Golgi stained neurons from juvenile WT, T4826I, CGG and DM mice

	Hippocampus			Cortex		
	Tests of fixed effects *P* values			Tests of fixed effects *P* values		
	Sex	Genotype	Sex*genotype	Sex	Genotype	Sex*genotype
Sholl plot profile analysis	0.9742	0.8776	0.2447	0.4072	0.7822	0.7118
Distance from Soma of peak intersection	0.1509	0.2735	*0.0573*	0.9732	**0.0266**	0.4988
Maximum number of intersections	0.1502	0.7137	0.485	0.4843	0.4136	0.767
Area under Sholl curve (AUC)	0.9029	0.9697	0.1482	0.7682	0.2435	0.5821
Proximal AUC	0.8411	0.8136	0.2795	0.6947	0.3062	0.6492
Distal AUC (log)	0.8003	0.9143	0.1638	0.9886	0.2965	0.2057
Primary dendrite number	0.1238	*0.0582*	0.1822	0.9567	0.6292	0.5545
Terminal tips	0.2072	**0.012**	*0.0558*	0.4867	**0.0138**	0.7882
Dendritic tips/dendrite	0.8615	0.1439	0.099	0.4641	**0.0002**	0.7604
Soma area	0.4441	**0.0012**	0.7326	0.8041	0.6098	0.9913
Sum dendritic length	0.7591	0.9532	0.0985	0.8427	0.0666	0.4839
Mean dendritic length	0.9998	0.3681	0.0817	0.8456	**0.0072**	0.5754
Sum dendritic intersections	0.8988	0.9696	0.1359	0.7692	0.2306	0.5761

Note: Numbers in bold font indicate p values < 0.05.

were limited to male neurons and included a significant increase in the distance from the soma of the maximum number of dendritic intersections in T4826I male neurons compared to either WT (P = 0.0028) or DM (P = 0.0128) neurons (Figure 1D,E, Table 2; Table S2). There were no significant differences between genotypes with respect to the maximum number of dendritic intersections (Figure 1F,G) or the total area under the Sholl curve (Figure 1H,I) in male or female hippocampal neurons.

While Sholl analysis provides a broad picture of dendritic complexity, it does not always show subtle yet relevant changes in dendritic architecture (Figure S1B). Therefore, we refined our analysis by further characterizing the number, complexity and length of dendrites in pyramidal CA1 hippocampal neurons. In male but not female hippocampal neurons, there was a significant decrease in the total number of primary dendrites in T4826I compared to WT (P = 0.0345) (Figure 2A,B, Table 2; Table S2). CGG male hippocampal neurons had a significantly increased number of primary dendrites compared to T4826I (P = 0.0055) and DM (P = 0.0476) male hippocampal neurons (Figure 2A,B, Table 2; Table S2). Mixed effects modeling showed a significant overall effect of genotype on the number of terminal dendritic tips ($F_{3,279}$ = 3.71, P = 0.012, Table 1). This was largely driven by an increased number of dendritic tips in CGG male hippocampal neurons compared to WT (P = 0.0005), T4826I (P = 0.0119) and DM (P = 0.0002) male neurons (Figure 2C,D, Table 2; Table S2). There was also a significant sex difference within CGG hippocampal neurons with male neurons having more dendritic tips compared to female CGG neurons (~20%, P = 0.0034) (Figure 2C,D). Significant differences in the number of dendritic tips per primary dendrite, a measure of dendritic complexity, were limited to an increased number of dendritic tips per primary dendrite in T4826I male compared to WT male hippocampal neurons (P = 0.0022) (Figure 2E,F, Table 2; Table S2). Within male neurons, mean dendritic length was significantly increased in T4826I compared to WT hippocampal neurons (P = 0.0252, Figure 2G,H, Table 2; Table S2, Supporting Information).

Mixed effect modeling showed a significant effect of genotype on the area of neuronal somata ($F_{3,40}$ = 6.45, P = 0.0012, Table 1) driven by a significantly increased soma area of CGG neurons by ~15-26% compared to the other genotypes (Figure 2I,J; Table S2). Unlike the dendritic parameters, both male and female hippocampal neurons exhibited genotype effects on soma area. Within males, the soma area of CGG neurons was significantly increased compared to T4826I (P = 0.035) and DM (P = 0.0073) hippocampal neurons (Figure 2I, Table 2; Table S2). Within females, the soma area of CGG neurons was significantly increased compared to WT (P = 0.0146), T4826I (P = 0.0302) and DM (P = 0.0042) hippocampal neurons (Figure 2I,J, Table 2; Table S2). Collectively, these data indicate that the T4826I and CGG mutations increase dendritic complexity in pyramidal CA1 hippocampal neurons, and do so more consistently in male *vs* female juvenile mice.

Sholl plots and representative images of the basilar dendritic arbor of Golgi-stained pyramidal neurons within the somatosensory cortex for each sex and genotype are shown in Figure 3A,C. In contrast to the observations of CA1 hippocampal neurons, genotype effects on dendrite morphology were seen in both sexes. Mixed effects model analysis showed a significant genotype effect on the distance from the soma of the maximum number of dendritic intersections ($F_{3,318}$ = 3.11, P = 0.0266, Table 1) driven by a significant increase in the distance from the soma of the maximum number of dendritic intersections in CGG (~13%, P = 0.0186) and DM (~12%, P = 0.0209) compared to WT cortical neurons (Table S2). Examining each sex individually, in males there was a significant increase in the distance from the soma of maximum dendritic intersections in CGG compared to WT neurons (P = 0.0443) (Figure 3D, Table 2; Table S2), while in females there was a significant increase in the distance from the soma of maximum dendritic intersections in CGG (P = 0.0411) and DM (P = 0.0260) compared to T4826I neurons (Figure 3E, Table 2; Table S2). The maximum number of dendritic intersections only differed in female neurons, with a significantly greater maximum number of dendritic intersections in CGG compared to T4826I female cortical

TABLE 2 Summary of significant effects of genotype on dendrite morphology

Brain region of neurons	Morphology parameter	Sex	Genotypes	Change from WT, %	Genotypes	Change from T4826I, %	Genotypes	Change from DM, %
Hippocampal	Distance from soma of peak # intersections (μm)	Male	WT vs T4826I	31.73% increase			DM vs 4826I	25.28% increase
Hippocampal	Number of primary dendrites/ neuron	Male	WT vs T4826I	20.68% decrease	T4826I vs CGG	35.35% increase	DM vs CGG	21.85% increase
Hippocampal	# Dendritic tips/neuron	Male	WT vs CGG	24.67% increase	T4826I vs CGG	17.72% increase	DM vs CGG	27.77% increase
Hippocampal	Tips/primary dendrite	Male	WT vs T4826I	46.49% increase				
Hippocampal	Mean dendritic length (μm)	Male	WT vs T4826I	41.23% increase				
Hippocampal	Soma area (μm^2)	Female	WT vs CGG	22.87 % increase	T4826I vs CGG	20.81% increase	DM vs CGG	27.5% increase
Hippocampal	Soma area (μm^2)	Male			T4826I vs CGG	18.89% increase	DM vs CGG	25.39% increase
Cortical	Distance from soma of peak # intersections (μm)	Female			T4826I vs CGG	16.36% increase		
					T4826I vs DM	17.5% increase		
Cortical	Distance from soma of peak # intersections (μm)	Male	WT vs CGG	16.75% increase				
Cortical	# Intersections at peak	Female			T4826I vs CGG	17.94% increase		
Cortical	Area under sholl curve	Female			T4826I vs DM	29.99% increase		
Cortical	Distal area under sholl cuve	Female	WT vs DM	22.84% increase				
Cortical	# Dendritic tips/neuron	Female	WT vs DM	19.79% increase	T4826I vs DM	23.03% increase		
Cortical	Tips/primary dendrite	Male	WT vs DM	17.22% increase	T4826I vs DM	18.42% increase		
Cortical	Tips/primary dendrite	Female	WT vs DM	32.07% increase	T4826I vs DM	23.38% increase		
			WT vs CGG	23.33% increase				
Cortical	Mean dendritic length (μm)	Female	WT vs DM	47.42% increase	T4826I vs DM	40.85% increase		

Abbreviations: CGG, mice expressing a CGG repeat expansion in the fragile X mental retardation 1 gene; DM, double mutation (CGG+T4826I); T4826I, T4826I-ryanodine receptor 1 mutation; WT, wild-type.

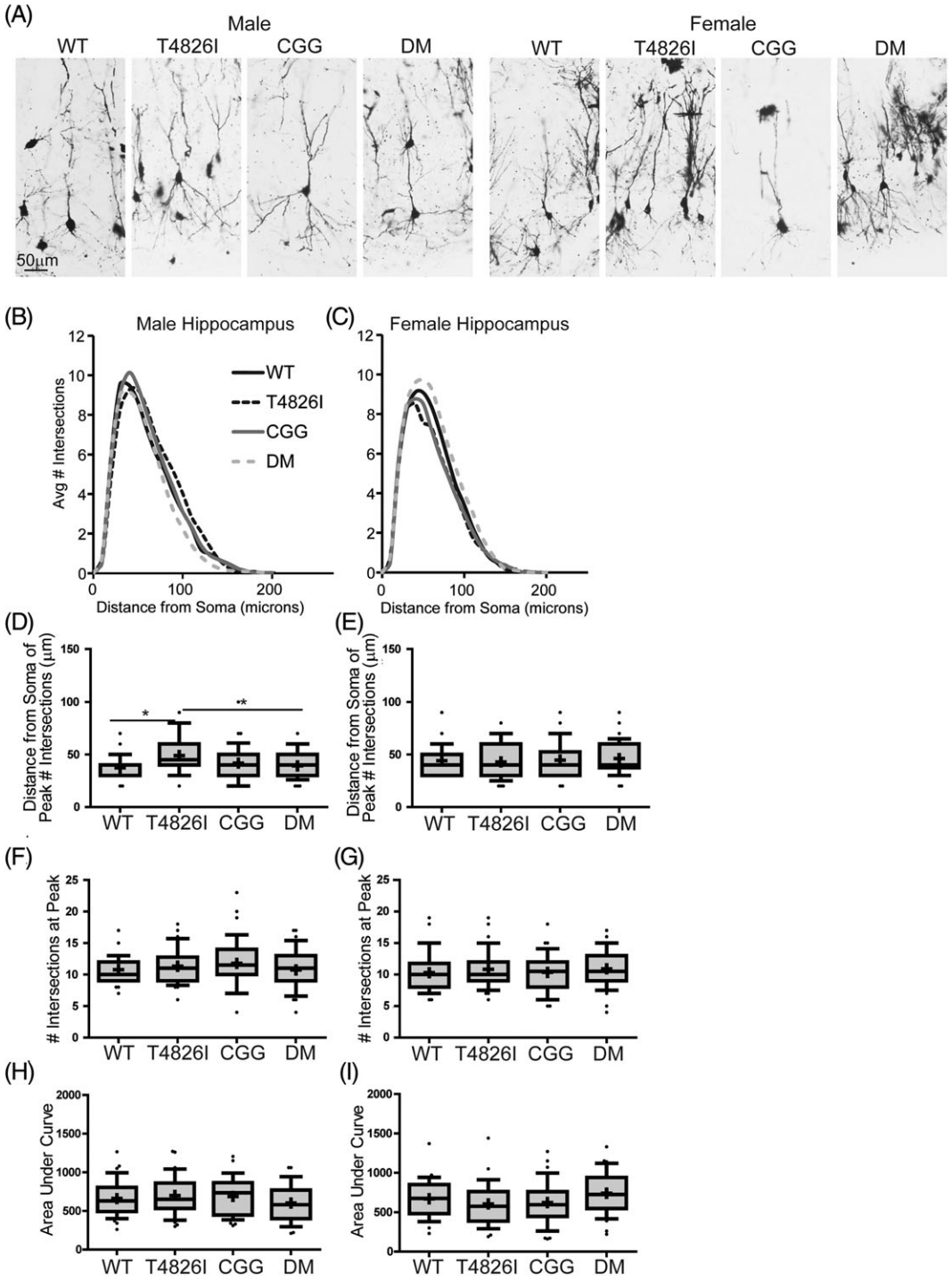

FIGURE 1 Genotype influences the dendritic morphology of pyramidal neurons in the CA1 hippocampus of juvenile male but not female mice. (A) Representative photomicrographs and (B, C) Sholl plots of the basilar dendritic arbors of Golgi-stained pyramidal CA1 hippocampal neurons derived from P 25-30 male and female WT, T4826I, CGG or DM mice. Dendritic morphology was further assessed by quantifying (D, E) the distance from the soma to the maximum number of dendritic intersections, (F, G) the maximum number of intersections, and (H, I) the total area under the curve of the Sholl plot (0-180 μm from the soma taken at 10 μm increments). Data are presented as box plots, "+" indicates the mean; whiskers, the 10-90th percentile, dots are outliers (n = 32-40 neurons per sex per genotype from at least six independent mice). Significant differences were determined using a mixed effects model. Asterisk indicates a significant difference between groups as determined by the differences of least squares means at $P \leq 0.05$

neurons (P = 0.0440) (Figure 3F,G, Table 2; Table S2). Genotype effects on the area under the Sholl curve were limited to female neurons with a significantly increased area under the Sholl curve in DM compared to T4826I (P = 0.0401) female cortical neurons (Figure 3H,I, Table 2; Table 2). Examining proximal vs distal changes in dendrite complexity, there were no genotype or sex differences in the proximal area under the curve (Table 1, results not shown); however, in female neurons only, there was a significant increase in distal half of the area under the curve in DM compared to WT (P = 0.0189) female cortical neurons (Figure 3J,K, Table 2; Table S2).

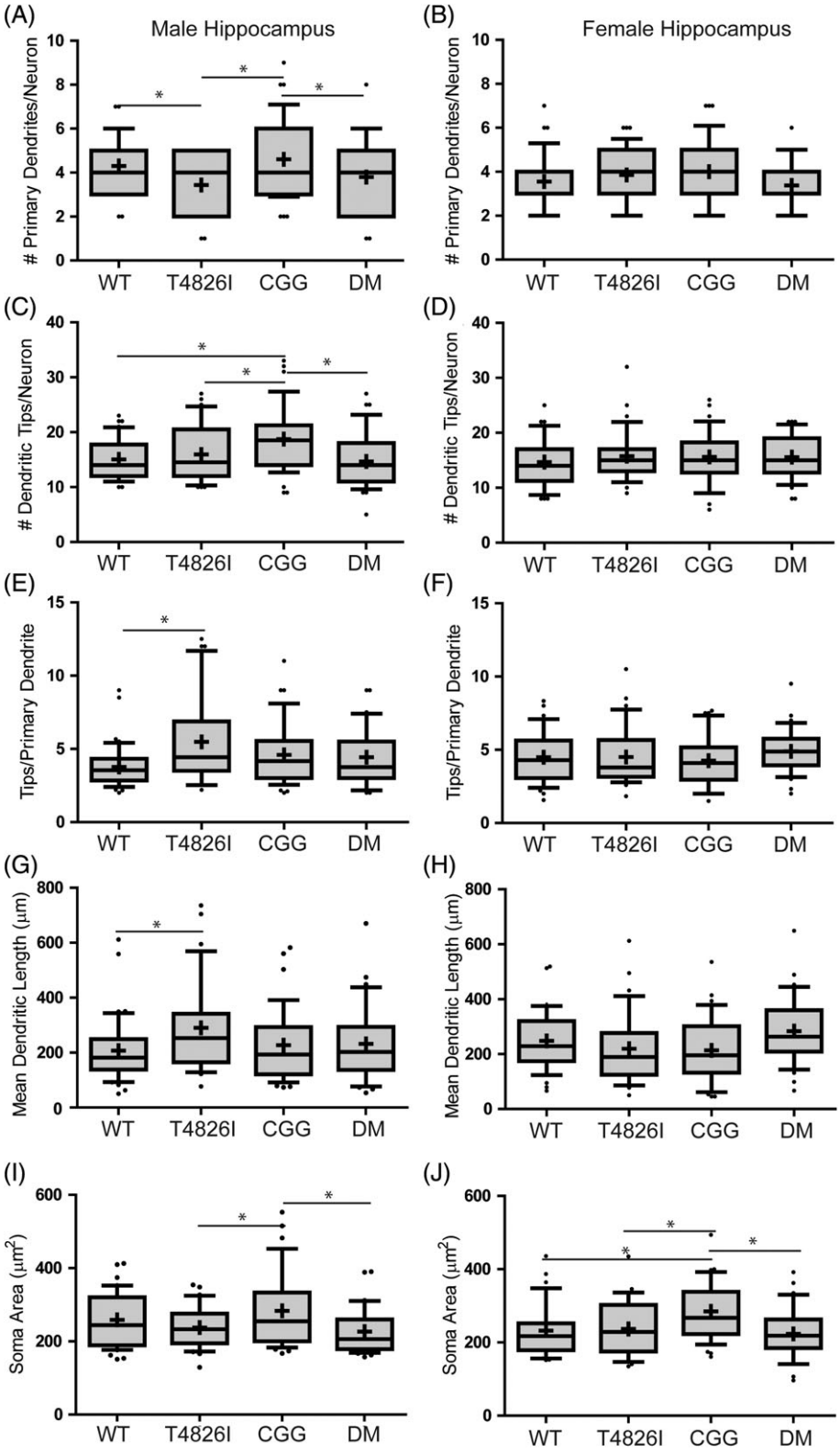

FIGURE 2 Genotype influences the dendritic morphology of pyramidal neurons in the CA1 hippocampus of juvenile male but not female mice, and increases the area of neuronal somata in both sexes. Basilar dendritic arbors in Golgi-stained pyramidal CA1 hippocampal neurons derived from P 25-30 male and female WT, T4826I, CGG or DM mice were assessed by quantifying (A, B) the number of primary dendrites per neuron, (C, D) the number of dendritic tips per neurons, (E, F) the number of dendritic tips per primary dendrite, (G, H) the mean length of all dendrites (total dendritic length/total dendrites per neuron, and (I, J) the area of the neuronal soma. Data are presented as box plots, "+" indicates the mean; whiskers, the 10-90th percentile, dots are outliers (n = 32-40 neurons per sex per genotype from at least six independent mice). Significant differences were determined using a mixed-effects model. Asterisk indicates a significant difference between groups as determined by the differences of least squares means at $P \leq 0.05$

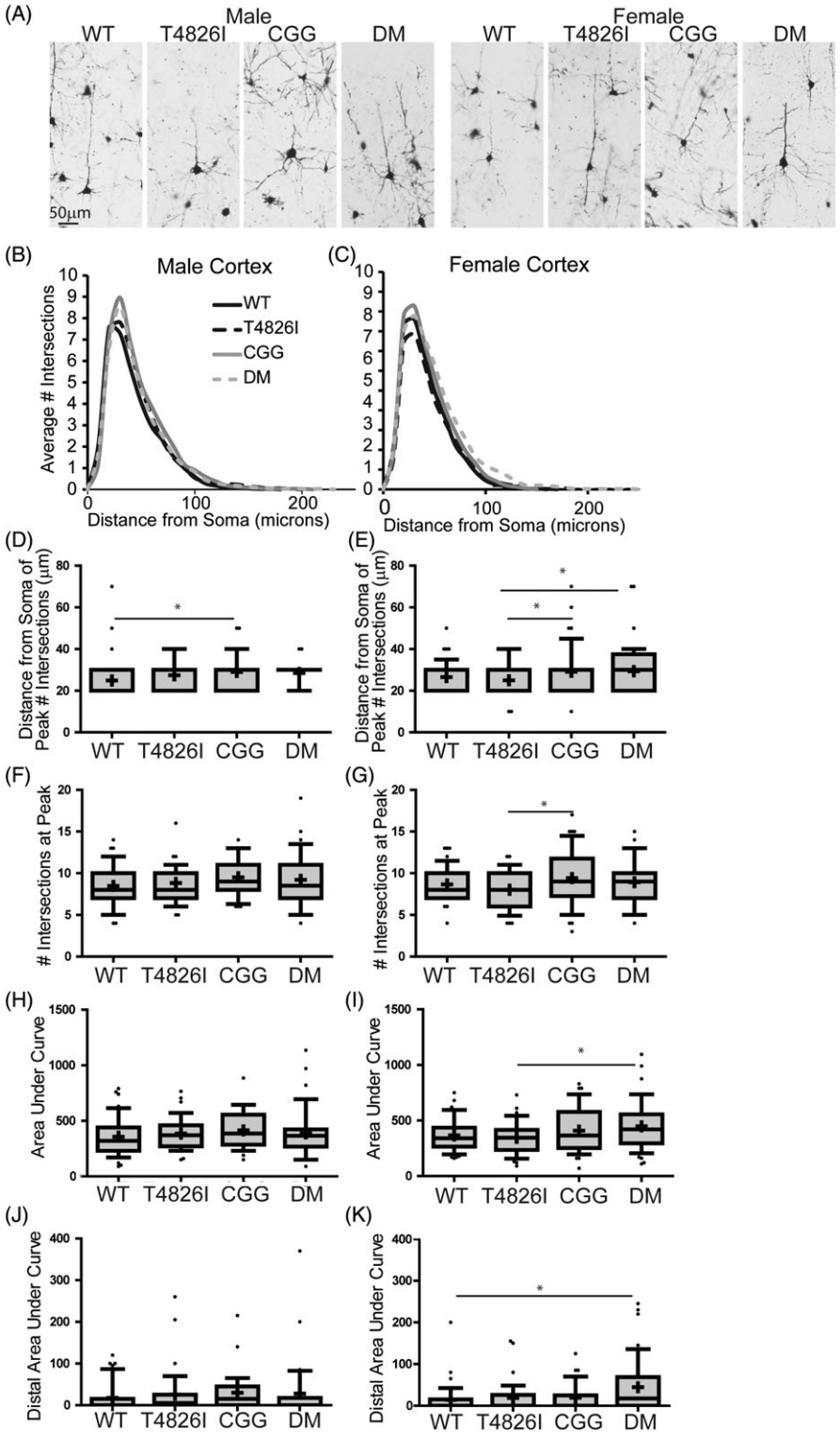

FIGURE 3 Genotype influences the dendritic morphology of pyramidal neurons in the somatosensory cortex of juvenile male and female mice. (A) Representative photomicrographs and (B, C) Sholl plots of the basilar dendritic arbors of Golgi-stained pyramidal somatosensory cortical neurons derived from P 25-30 male and female WT, T4826I, CGG or DM mice. Dendritic morphology was assessed by quantifying (D, E) the distance from the soma to the maximum number of dendritic intersections, (F, G) the maximum number of intersections, (H, I) the total area under the curve of the Sholl plots (0-180 μm from the soma taken at 10 μm increments), and (J, K) the distal area under the Sholl curve (90-180 μm from the soma). Data are presented as box plots, "+" indicates the mean; whiskers, the 10-90th percentile, dots are outliers (n = 32-48 neurons per sex per genotype from at least six independent mice). Significant differences were determined using a mixed-effects model. Asterisk indicates a significant difference between groups as determined by the differences of least squares means at $P \leq 0.05$

We further characterized the number, complexity and length of dendrites in cortical neurons derived from male and female mice of each genotype. In contrast to hippocampal neurons, there were no genotype differences in the number of primary dendrites extended by cortical neurons in either sex (Figure 4A,B). Mixed effects model analysis showed a significant genotype effect for the number of terminal dendritic tips ($F_{3,45.2}$ = 3.95, P = 0.0138, Table 1) driven by increases in CGG (~16%, P = 0.0175) and DM (~16%, P = 0.0178) neurons compared to WT neurons, as well as increases in CGG (~16%, P = 0.0202) and DM neurons (~16%, P = 0.0205) compared to T4826I neurons (Table S2). Examining genotype effects within each sex, significant differences were limited to female neurons, with an increase in number of dendritic tips in DM compared to WT (P = 0.0326) or T4826I (P = 0.0183) female cortical neurons (Figure 4D, Table 2, Table S2). There was also a significant overall genotype effect on the number of dendritic tips per primary dendrite ($F_{3,41}$ = 8.11, P = 0.0002, Table 1), again driven by increased values for CGG (~20%, P = 0.0022) and DM (~24%, P = 0.0002) compared to WT cortical neurons, as well as increased values for CGG (~16%, P = 0.0096) and DM neurons (~21%, P = 0.0010) compared to T4826I cortical neurons (Table S2). Within males, the number of dendritic tips per dendrite was significantly increased in DM compared to WT (P = 0.0428) or T4826I (P = 0.0379) cortical neurons (Figure 4E, Table 2; Table S2). Within females, the number of dendritic tips per dendrite was significantly increased in CGG (P = 0.0098) and DM (P = 0.0005) compared to WT cortical neurons, and in DM compared to T4826I (P = 0.0066) cortical neurons (Figure 4F, Table 2; Table S2). There was also an overall effect of genotype on mean dendritic length ($F_{3,276}$ = 4.10, P = 0.0072, Table 1) driven by increased mean dendritic length in CGG (~24%, P = 0.0357) and DM (~34%, P = 0.0022) compared to WT cortical neurons, and increased mean dendritic length in DM compared to T4826I (~28%, P = 0.0105) cortical neurons (Table 2). Examining each sex, significant effects were limited to female neurons, with DM female neurons having greater mean dendritic length compared to WT (P = 0.0025) or T4826I (P = 0.0078) female neurons (Figure 4H, Table 2; Table S2). Unlike hippocampal neurons, no significant effects of genotype or sex on soma area were detected in cortical neurons (Figure 4I,J).

3.2 | Genotype impacts the social behavior of juvenile mice

In order to determine whether genotype-dependent changes in dendritic morphology are associated with changes in behavior, we used the three-chambered social approach task to assess social behavior in juvenile mice of each genotype. This test was chosen because it is a simple, automated and standardized assay that can be used with juvenile animals.[44–46,64] Mice were initially allowed to explore the empty left and right chambers during a 10 minutes habituation period. There were no significant differences in the combined number of side entries or velocity of the mice during the habituation phase for any of the genotypes or sexes (results not shown).

During the sociability phase, typical approach behavior was defined as spending significantly more time with a mouse vs the object. Time spent in the center chamber is shown in graphs for illustrative purpose only.[47] Genotype impacted sociability in both male and female mice. WT (t(20) = 3.138, P = 0.0052) and CGG (t(16) = 2.497, P = 0.0238) male mice spent more time in the chamber containing a mouse *vs* an object (Figure 5A); however, T4826I and DM male mice failed to show a preference (Figure 5A). Similarly, WT (U = 52, P = 0.0128) and CGG (t(20) = 6.165, P = 0.0001) female mice spent significantly more time in the chamber containing a mouse vs an object (Figure 5B). T4826I female mice trended toward being social; however, the time spent in the chamber with the mouse vs object was not statistically significant (P = 0.09). DM female mice also failed to show a preference (Figure 5B). We next examined the more stringent social criteria of time spent in close proximity (≤ 1 in. to the object vs the mouse. WT (t(20) = 4.709, P = 0.0001) and CGG (t(16) = 3.101, P = 0.0069) male mice spent significantly more time in close proximity to a mouse vs an object, while T4826I and DM male mice failed to show a preference (Figure 5C). Amongst female mice, the time spent in close proximity to a mouse vs an object was significantly increased in WT (t(28) = 2.197, P = 0.0364) and CGG (t(13) = 7.349, P = 0.0001) female mice but not in T4826I or DM female mice (Figure 5D). There was also a significant effect of genotype on the time spent in close proximity to the mouse (sex $F_{(1,82)}$ = 0.00, P = 0.952; *genotype* $F_{(3,82)}$ = 10.01 P = 0.0001; interaction $F_{(3,82)}$ = 2.57, P = 0.0596, two way ANOVA with Tukey's multiple comparison test), with this variable decreased most significantly in the DM compared to WT, T4826I and CGG genotypes (Figure 5C,D). Velocity of mice during the testing phase was similar between genotypes in both sexes (Figure 5E,F). Additionally, there were no differences in body mass (Figure S2). Collectively, these results indicate that genotype impacts social behavior as assessed by the three-chambered social approach task.

4 | DISCUSSION

Genetic studies have identified a strong association between heritable mutations in Ca^{2+} signaling and increased risk for NDDs.[9,11] Here, we examined the effects of two mutations associated with dysregulated Ca^{2+} signaling in neurons, the T4826I-*RYR1* gain-of-function mutation and the *FMR1* premutation, on NDD-relevant outcomes in a preclinical model of late childhood/early adolescence. This study showed that these mutations, alone or in combination, enhanced dendritic arborization in a brain region and sex-specific manner, and impaired social behavior. Specifically, we observed that: (a) the dendritic morphology of pyramidal CA1 hippocampal neurons was altered in male but not female mice with the greatest number of differences relative to WT observed in T4826I males; (b) the dendritic morphology of pyramidal neurons in the somatosensory cortex was altered in both male and female mice, increases in dendritic complexity were observed in CGG and DM males, but the most robust increases in dendritic complexity were seen in DM females; and (c) genotype impacted performance of juvenile mice in the three chambered social approach task.

While we cannot conclude that the observed changes in dendrite morphology observed here occur through altered calcium dynamics, previously published data support the hypothesis that calcium signaling is dysregulated in both the T4826I-*RYR1* gain-of-function mutation and FMR1 premutation mouse models. RYRs, as a class of

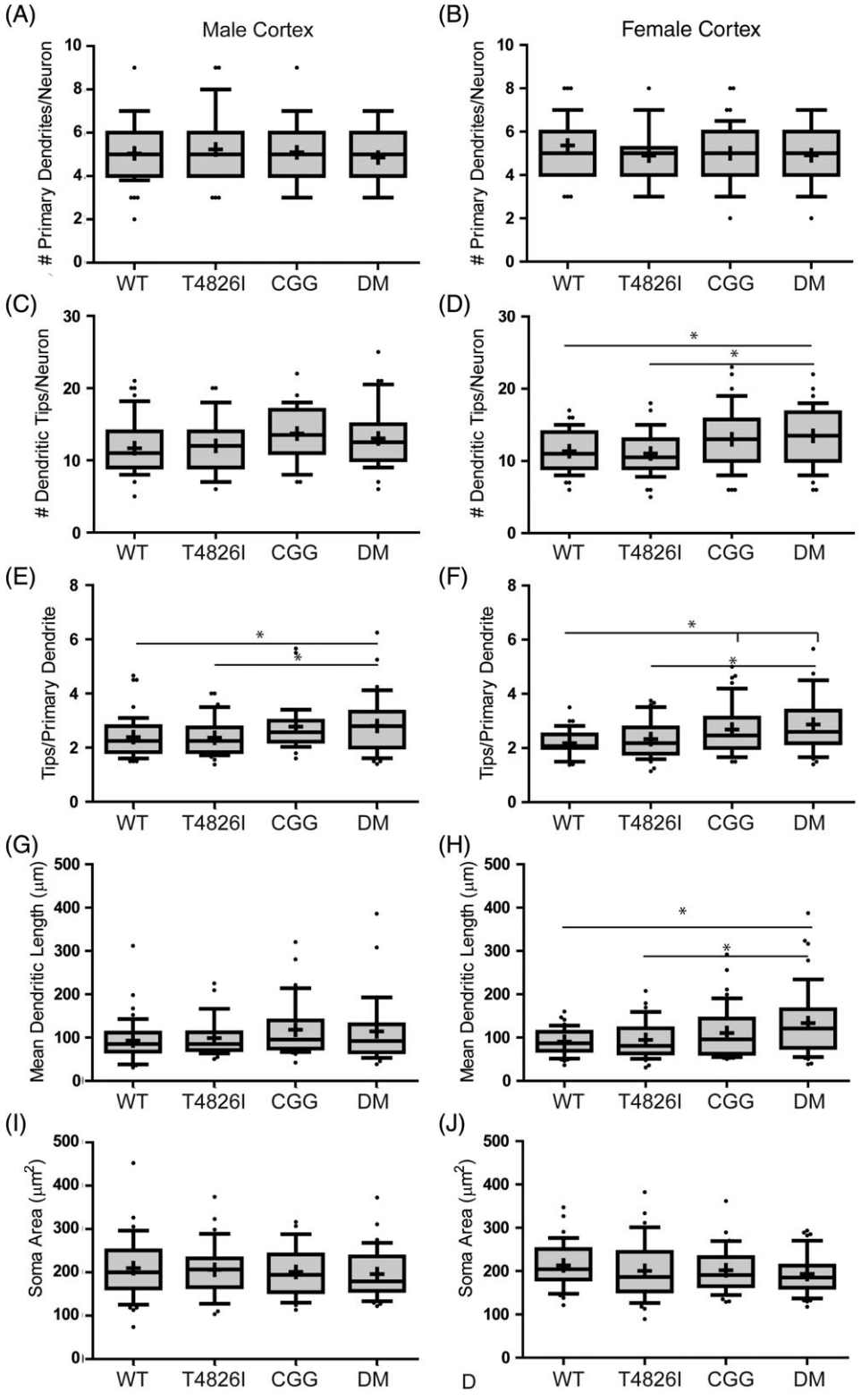

FIGURE 4 Genotype influences the dendritic morphology of pyramidal neurons in the somatosensory cortex of juvenile male and female mice but has no effect on the area of neuronal somata in either sex. Basilar dendritic arbors in Golgi-stained pyramidal somatosensory cortical neurons derived from P 25-30 male and female WT, T4826I, CGG or DM mice were assessed by quantifying (A, B) the number of primary dendrites per neuron, (C, D) the number of dendritic tips per neuron, (E, F) the number of dendritic tips per primary dendrite, (G, H) mean dendritic length per neuron, and (I, J) neuronal soma area. Data are presented as box plots, "+" indicates the mean; whiskers, the 10-90th percentile, dots are outliers (n = 32-48 neurons per sex per genotype from at least six independent mice). Significant differences were determined using a mixed-effects model. Asterisk indicates a significant difference between groups as determined by the differences of least squares means at $P \leq 0.05$

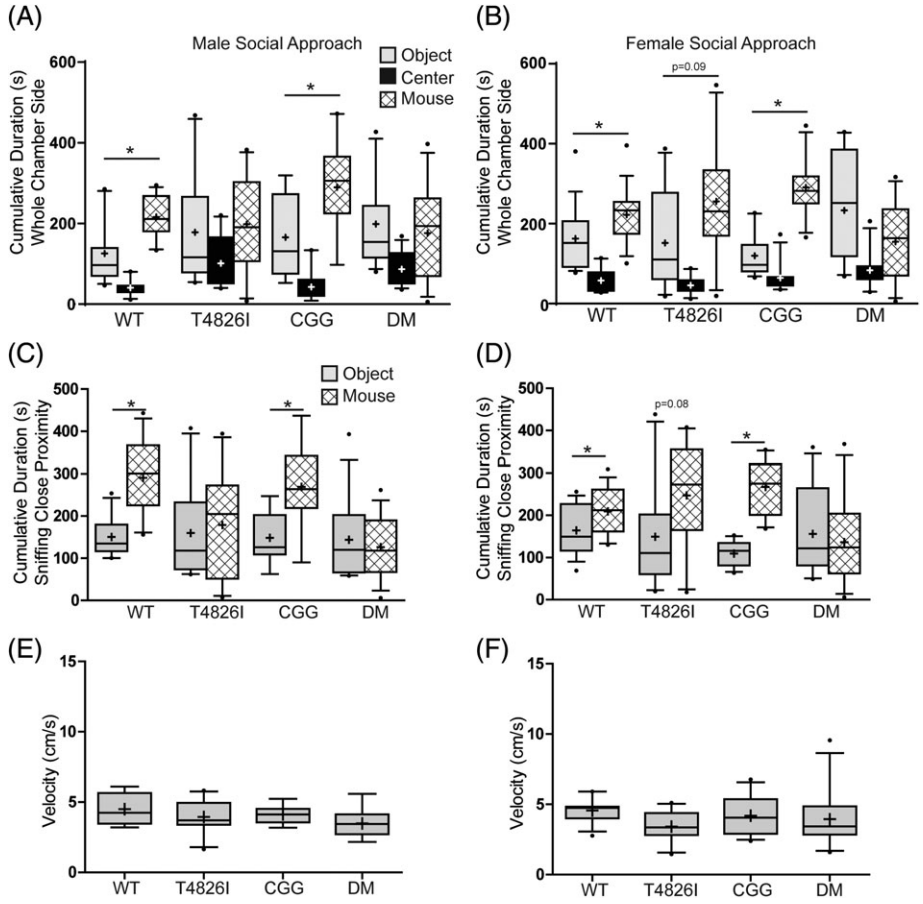

FIGURE 5 Genotype influences sociability by three chambered approach in juvenile male and female mice. Juvenile WT, T4826I, CGG or DM mice of both sexes were allowed to explore a three-chambered social approach arena with one side containing a novel object and the other a novel mouse for a 10 minutes period and assessed for (A, B) the cumulative time spent in the chamber with the object vs mouse, (C, D) the cumulative time spent in close proximity (≤1 in. to the object or mouse, and (E, F) the velocity of mice over the entire testing period. Data are presented as box plots, "+" indicates the mean; whiskers, the 10-90th percentile, dots are outliers (male/female n = 11/15 WT, 10/10 T4826I, 9/11 CGG, 13/11 DM animals each from at least six independent litters). Sociability was defined as spending more time with the mouse vs the object. Time spent in the center chamber (A, B) is shown for illustrative purposes only. Significant differences were determined using Student's t test for parametric data and Mann-Whitney U test for nonparametric data (A-D) and by one-way ANOVA followed by Newman-Keuls multiple comparison test for parametric data (E) or Kruskal Wallis followed by Dunn's multiple comparison tests for nonparametric data (F)

intracellular calcium ion channels, are essential in regulating calcium release, and the T4826I-*RYR1* gain of function mutation in mice has been shown to elevate intracellular calcium levels in muscle.[21] While not as obvious as RYR gain-of-function neurons, FMR1 premutation neurons also provide evidence of disrupted calcium signaling. FMRP has been shown to bind and regulate ion channel expression in addition to altering the function of calcium binding proteins.[65,66] Elevated Ca^{2+} concentrations and abnormal patterns of spontaneous Ca^{2+} oscillations have been reported in central neurons and astrocytes,[29,30] *Drosophila*,[66] human iPSC-derived neurons from FMR1 premutation patients[42] and in human fibroblasts with CGG repeats in the FMR1 gene.[67] Furthermore, in human fibroblasts with FMR1 CGG repeats, pharmacological destabilization of CGG repeat RNA restores calcium dynamics.[67] Juvenile *Fmr1−/−* mice have elevated synchrony in the firing of cortical neurons as indicated by *in vivo* calcium imaging, especially during the first two postnatal weeks.[68,69] Together these results highlight elevated calcium signaling as a convergent pathway of both T4826I-*RYR1* gain-of-function mutation and CGG models. Given the importance of calcium signaling in dendritic morphology and connectivity, it is possible that altered calcium signaling contributes to the effect on dendritic morphology of each genetic mutation observed in this study.

Previous studies have examined dendritic arborization and social behavior in adult *FMR1* premutation mice. In adult male *FMR1* premutation (156 CGG repeats) mice, pyramidal neurons in the primary visual cortex are reduced in branching complexity and dendritic length compared to age- and sex-matched WT.[38] Decreased dendritic complexity was also reported for basilar dendrites of pyramidal neurons in the medial prefrontal cortex and CA3 hippocampus of *FMR1* premutation mice.[70] In contrast, the differences in juvenile CGG mice relative to age- and sex-matched WT mice were few but consisted of increased dendritic complexity. The discrepancy between these studies likely reflects differences in the adult vs juvenile brain, suggesting that genotype effects on dendritic arborization in the juvenile brain—a time of active dendritic growth and remodeling—are not predictive of genotype effects on dendritic morphology in the adult brain. Perhaps not surprisingly, the subtle changes in dendritic arborization observed in the CGG juvenile mice were not associated with altered social

behavior. Similarly, adult *FMR1* premutation mice behave no differently than WT mice in social interaction and social novelty tasks.[70] CGG hippocampal neurons also exhibited increased soma area. Soma size has been shown to change significantly over postnatal development in rat supraoptic magnocellular neurons.[71] Soma size is influenced by calcium signaling, as evidenced by reports that pharmacological antagonism of Q-type or AMPA/kainite calcium channels decreases soma size in rat ganglion cells.[72] While the mechanisms underlying altered soma size in our models remains to be determined, these data suggest that calcium signaling may be involved.

While age-related changes in RyR function were recently showed to impair cognition in adult mouse models of Alzheimer's disease,[73] this study provides the first characterization of juvenile mice with genetically altered RyR function. The T4826I and DM mouse models showed that expression of these mutations generally enhanced dendritic arborization, although the outcome varied as a function of sex and brain region. This is consistent with previous *in vitro* studies demonstrating that environmental stressors with a "gain-of-function" effect on RyR1 similarly increase dendritic arborization of hippocampal and cortical neurons.[27,74,75] Genotype effects on dendritic arborization mapped onto deficits in social behavior. Increased dendritic complexity was observed in the CA1 hippocampus of T4826I males, and in the somatosensory cortex of DM males and females, which were the same experimental groups that exhibited the most significant deficits in social approach.

While our data do not establish a cause-effect relationship between increased dendritic arborization and impaired social behavior, they add to emerging evidence linking these two phenomena in juvenile animals. For example, early life stress caused by maternal separation increased apical dendritic branch number and length of pyramidal neurons in the medial prefrontal cortex of female juvenile rats, and these morphological outcomes coincided with deficits in social interactions.[76] Similarly, in a model of endoplasmic reticulum stress, adult male mice exhibit decreased social behavior coincident with hyperconnectivity in the neural circuit from the medial prefrontal cortex to the dorsal hippocampus as measured by implanted depth electrodes.[61] However, our results also indicate that alterations in dendritic morphology do not necessarily predict behavioral outcomes or vice versa. We found no difference in social behavior between WT and CGG juvenile mice despite evidence of subtle differences in dendritic morphology. Alternatively, the lack of association between altered dendritic morphology and social behavior in the CGG mouse may indicate that the changes in dendritic morphology in this mouse model were below the "threshold" required to manifest as behavioral deficits.

A key question raised by this study is whether co-expression of the T4826I-*RYR1* mutation and *FMR1* premutation amplified the impact of either mutation alone. With respect to dendritic arborization of hippocampal neurons, significant differences relative to WT were observed in male CGG and T4826I but not DM mice. Thus, there appears to be no interaction between the genotypes that enhances outcome in hippocampal neurons. However, in cortical neurons, there were subtle dendritic effects in the CGG mice alone but robust effects in the DM compared to WT in both sexes, but especially in females, which included a 32% increase in dendritic tips/primary dendrite and a 47% increase in mean dendritic length. Furthermore, in cortical neurons a number of parameters of dendritic complexity were significantly increased in DM compared to T4826I neurons including an 18% increase in dendritic tips/primary dendrite in male neurons, a 30% and 41% increase in area under the curve and mean dendritic length, respectively, in female neurons. These data suggest that co-expression of these mutations does amplify the effect of either mutation alone on dendritic morphology of cortical neurons in both sexes. With respect to social behavior, both male and female DM mice exhibit social deficits. This phenotype appears to be driven by the T4826I-*RYR1* mutation because male and female CGG mice exhibit normal social approach, while T4826I mice exhibit impaired social approach, although both male and female T4826I mice were trending toward normal sociability. Further work involving more nuanced social behavioral assays, like dyadic play and ultrasonic calls during social interactions are required to dissect and confirm the influence of each gene on mouse social behavior.

Unraveling the complex etiology of NDDs is an ongoing challenge, and understanding the mechanisms by which susceptibility genes interact with each other and environmental risk factors to determine individual risk remains a critical data gap in the field. While we cannot rule out other mechanisms, our findings together with previous studies linking these mutations to altered calcium signaling,[21,65] suggest models expressing distinct heritable mutations that modify Ca^{2+} signaling early in life may be capable of altering neural circuits by interfering with normal patterns of dendritic arborization, and these changes may contribute to functional deficits in NDD-relevant behaviors. Importantly, histological studies of brains from patients diagnosed with ASD[77] or fragile X syndrome[78] have showed significantly increased dendritic complexity relative to neurotypical controls. Moreover, the magnitude of change in dendritic arborization we observed in the mouse models, which ranged from ~17% to 47% increase in dendritic complexity compared to sex-matched WT controls, is within the range of clinical data indicating a 15% increase in local connectivity in the brains of autistic patients vs neurotypical controls based on fMRI imaging.[20]

While we cannot rule out other mechanisms, our data are consistent with the hypothesis that Ca^{2+} signaling represents a convergence point for multiple genetic factors, which if they drive Ca^{2+} signaling in the same direction, as is the case with the T4826I-*RYR1* mutation and *FMR1* premutation, can amplify phenotypic outcomes. Importantly, our data also suggest that human gain of function mutations in *RYR1* linked to MHS[10,24] have effects on not only skeletal muscle, but also neurons. These data extend previous reports of ion channel deficits in autism,[79] the localization of at least one *RYR* isoform on chromosome 15q, a region associated with autism susceptibility genes,[80] and identification of RYR2 as a potential ASD risk gene.[81] However, it should be noted that humans with the *RYR1* gain of function mutation are typically heterozygous, unlike the homozygous T4826I-*RYR1* mice used in this study. It is possible that the phenotype we observed in the mouse may be more pronounced than what is observed in humans. However, like the human condition, the T4826I mouse exhibits no overt clinical pathogenic phenotype.[22] Identifying genetic and environmental risk factors that interact with gain-of-function *RYR* mutations and/or *FMR1*

premutation to increase individual risk for NDDs remains to be determined, and the three genetic models characterized here will serve as powerful tools for addressing this critical question.

ACKNOWLEDGMENTS

The authors wish to thank Susan Hulsizer (University of California, Davis) for assistance with obtaining breeders for each of the genetic lines. This work was supported by the National Institutes of Environmental Health Sciences (grants ES014901, ES011269 to PJL and INP, and T32 ES007059-funded predoctoral fellowship to SS), the Eunice Kennedy Shriver National Institute of Child Health & Human Development of the National Institutes of Health (grant F32 HD088016 to KPK), the Floyd and Mary Schwall Medical Research Fellowship Program (predoctoral fellowship to SS), and the United States Environmental Protection Agency (grant R833292 to PJL and INP). This project used core facilities supported by the MIND Institute Intellectual and Developmental Disabilities Research Center (grant U54 HD079125) and the National Institutes of Health National Center for Advancing Translational Sciences (grant UL1 TR000002). The content is solely the responsibility of the authors and does not necessarily represent the official views of the NIH or the USEPA. Furthermore, the NIH and USEPA did not endorse the purchase of any commercial products or services mentioned in the publication.

CONFLICTS OF INTEREST

All authors declare no potential conflicts of interest.

ORCID

Kimberly P. Keil https://orcid.org/0000-0002-7006-9420

REFERENCES

1. CDC. Prevalence of autism spectrum disorder among children aged 8 years—autism and developmental disabilities monitoring network, 11 sites, United States, 2010. *Cent Dis Control Prev MMWR*. 2014;6e3:1-13.
2. Lavelle TA, Weinstein MC, Newhouse JP, Munir K, Kuhlthau KA, Prosser LA. Economic burden of childhood autism spectrum disorders. *Pediatrics*. 2014;133:e520-e529.
3. Herbert MR. Contributions of the environment and environmentally vulnerable physiology to autism spectrum disorders. *Curr Opin Neurol*. 2010;23:103-110.
4. Landrigan PJ, Lambertini L, Birnbaum LS. A research strategy to discover the environmental causes of autism and neurodevelopmental disabilities. *Environ Health Perspect*. 2012;120:a258-a260.
5. Lyall K, Croen L, Daniels J, et al. The changing epidemiology of autism Spectrum disorders. *Annu Rev Public Health*. 2017;38:81-102.
6. Aldinger KA, Plummer JT, Qiu S, Levitt P. SnapShot: genetics of autism. *Neuron*. 2011;72(418–8):e1.
7. El-Fishawy P, State MW. The genetics of autism: key issues, recent findings, and clinical implications. *Psychiatr Clin North Am*. 2010;33:83-105.
8. Geschwind DH. Genetics of autism spectrum disorders. *Trends Cogn Sci*. 2011;15:409-416.
9. Krey JF, Dolmetsch RE. Molecular mechanisms of autism: a possible role for Ca2+ signaling. *Curr Opin Neurobiol*. 2007;17:112-119.
10. Pessah IN, Cherednichenko G, Lein PJ. Minding the calcium store: ryanodine receptor activation as a convergent mechanism of PCB toxicity. *Pharmacol Ther*. 2010;125:260-285.
11. Stamou M, Streifel KM, Goines PE, Lein PJ. Neuronal connectivity as a convergent target of gene x environment interactions that confer risk for autism Spectrum disorders. *Neurotoxicol Teratol*. 2013;36:3-16.
12. Chen JL, Nedivi E. Neuronal structural remodeling: is it all about access? *Curr Opin Neurobiol*. 2010;20:557-562.
13. Cline HT. Dendritic arbor development and synaptogenesis. *Curr Opin Neurobiol*. 2001;11:118-126.
14. Konur S, Ghosh A. Calcium signaling and the control of dendritic development. *Neuron*. 2005;46:401-405.
15. Redmond L, Ghosh A. Regulation of dendritic development by calcium signaling. *Cell Calcium*. 2005;37:411-416.
16. Alaerts K, Swinnen SP, Wenderoth N. Sex differences in autism: a resting-state fMRI investigation of functional brain connectivity in males and females. *Soc Cogn Affect Neurosci*. 2016;11:1002-1016.
17. Bourgeron T. A synaptic trek to autism. *Curr Opin Neurobiol*. 2009;19:231-234.
18. Delorme R, Ey E, Toro R, Leboyer M, Gillberg C, Bourgeron T. Progress toward treatments for synaptic defects in autism. *Nat Med*. 2013;19:685-694.
19. Keown CL, Shih P, Nair A, Peterson N, Mulvey ME, Muller RA. Local functional overconnectivity in posterior brain regions is associated with symptom severity in autism spectrum disorders. *Cell Rep*. 2013;5:567-572.
20. Supekar K, Uddin LQ, Khouzam A, et al. Brain hyperconnectivity in children with autism and its links to social deficits. *Cell Rep*. 2013;5:738-747.
21. Barrientos GC, Feng W, Truong K, et al. Gene dose influences cellular and calcium channel dysregulation in heterozygous and homozygous T4826I-RYR1 malignant hyperthermia-susceptible muscle. *J Biol Chem*. 2012;287:2863-2876.
22. Yuen B, Boncompagni S, Feng W, et al. Mice expressing T4826I-RYR1 are viable but exhibit sex- and genotype-dependent susceptibility to malignant hyperthermia and muscle damage. *FASEB J*. 2012;26:1311-1322.
23. Kim JH, Jarvik GP, Browning BL, et al. Exome sequencing reveals novel rare variants in the ryanodine receptor and calcium channel genes in malignant hyperthermia families. *Anesthesiology*. 2013;119:1054-1065.
24. Dlamini N, Voermans NC, Lillis S, et al. Mutations in RYR1 are a common cause of exertional myalgia and rhabdomyolysis. *Neuromuscul Disord*. 2013;23:540-548.
25. Adasme T, Haeger P, Paula-Lima AC, et al. Involvement of ryanodine receptors in neurotrophin-induced hippocampal synaptic plasticity and spatial memory formation. *Proc Natl Acad Sci USA*. 2011;108:3029-3034.
26. Lesiak A, Zhu M, Chen H, et al. The environmental neurotoxicant PCB 95 promotes synaptogenesis via ryanodine receptor-dependent miR132 upregulation. *J Neurosci*. 2014;34:717-725.
27. Wayman GA, Yang D, Bose DD, et al. PCB-95 promotes dendritic growth via ryanodine receptor-dependent mechanisms. *Environ Health Perspect*. 2012b;120:997-1002.
28. Cao Z, Hulsizer S, Cui Y, et al. Enhanced asynchronous Ca(2+) oscillations associated with impaired glutamate transport in cortical astrocytes expressing Fmr1 gene premutation expansion. *J Biol Chem*. 2013;288:13831-13841.
29. Cao Z, Hulsizer S, Tassone F, et al. Clustered burst firing in FMR1 premutation hippocampal neurons: amelioration with allopregnanolone. *Hum Mol Genet*. 2012;21:2923-2935.
30. Robin G, Lopez JR, Espinal GM, Hulsizer S, Hagerman PJ, Pessah IN. Calcium dysregulation and Cdk5-ATM pathway involved in a mouse model of fragile X-associated tremor/ataxia syndrome. *Hum Mol Genet*. 2017;26:2649-2666.
31. Willemsen R, Hoogeveen-Westerveld M, Reis S, et al. The FMR1 CGG repeat mouse displays ubiquitin-positive intranuclear neuronal inclusions; implications for the cerebellar tremor/ataxia syndrome. *Hum Mol Genet*. 2003;12:949-959.
32. Chonchaiya W, Au J, Schneider A, et al. Increased prevalence of seizures in boys who were probands with the FMR1 premutation and comorbid autism spectrum disorder. *Hum Genet*. 2012;131:581-589.

33. Hagerman R, Au J, Hagerman P. FMR1 premutation and full mutation molecular mechanisms related to autism. *J Neurodev Disord*. 2011;3: 211-224.
34. Hagerman R, Hagerman P. Advances in clinical and molecular understanding of the FMR1 premutation and fragile X-associated tremor/ataxia syndrome. *Lancet Neurol*. 2013;12:786-798.
35. Hagerman R, Lauterborn J, Au J, Berry-Kravis E. Fragile X syndrome and targeted treatment trials. *Results Probl Cell Differ*. 2012;54: 297-335.
36. Tassone F, Iong KP, Tong TH, et al. FMR1 CGG allele size and prevalence ascertained through newborn screening in the United States. *Genome Med*. 2012;4:100.
37. Berman RF, Buijsen RA, Usdin K, et al. Mouse models of the fragile X premutation and fragile X-associated tremor/ataxia syndrome. *J Neurodev Disord*. 2014;6:25.
38. Berman RF, Murray KD, Arque G, Hunsaker MR, Wenzel HJ. Abnormal dendrite and spine morphology in primary visual cortex in the CGG knock-in mouse model of the fragile X premutation. *Epilepsia*. 2012;53(Suppl 1):150-160.
39. Berman RF, Willemsen R. Mouse models of fragile X-associated tremor ataxia. *J Invest Med*. 2009;57:837-841.
40. Cunningham CL, Martinez Cerdeno V, Navarro Porras E, et al. Premutation CGG-repeat expansion of the Fmr1 gene impairs mouse neocortical development. *Hum Mol Genet*. 2011;20:64-79.
41. Chen Y, Tassone F, Berman RF, et al. Murine hippocampal neurons expressing Fmr1 gene premutations show early developmental deficits and late degeneration. *Hum Mol Genet*. 2010;19:196-208.
42. Liu J, Koscielska KA, Cao Z, et al. Signaling defects in iPSC-derived fragile X premutation neurons. *Hum Mol Genet*. 2012;21:3795-3805.
43. Yang M, Lewis F, Foley G, Crawley JN. In tribute to bob Blanchard: divergent behavioral phenotypes of 16p11.2 deletion mice reared in same-genotype versus mixed-genotype cages. *Physiol Behav*. 2015; 146:16-27.
44. Copping NA, Christian SGB, Ritter DJ, et al. Neuronal overexpression of Ube3a isoform 2 causes behavioral impairments and neuroanatomical pathology relevant to 15q11.2-q13.3 duplication syndrome. *Hum Mol Genet*. 2017;26:3995-4010.
45. Dhamne SC, Silverman JL, Super CE, et al. Replicable in vivo physiological and behavioral phenotypes of the Shank3B null mutant mouse model of autism. *Mol Autism*. 2017;8:26.
46. Gompers AL, Su-Feher L, Ellegood J, et al. Germline Chd8 haploinsufficiency alters brain development in mouse. *Nat Neurosci*. 2017;20: 1062-1073.
47. Yang M, Silverman JL, Crawley JN. Automated three-chambered social approach task for mice. *Curr Protoc Neurosci*. 2011; Chapter 8, Unit 8.26. doi:10.1002/0471142301.ns0826s56.
48. Keil KP, Sethi S, Wilson MD, Chen H, Lein PJ. In vivo and in vitro sex differences in the dendritic morphology of developing murine hippocampal and cortical neurons. *Sci Rep*. 2017;7:8486.
49. Wilson MD, Sethi S, Lein PJ, Keil KP. Valid statistical approaches for analyzing sholl data: mixed effects versus simple linear models. *J Neurosci Methods*. 2017;279:33-43.
50. Lein PJ, Yang D, Bachstetter AD, et al. Ontogenetic alterations in molecular and structural correlates of dendritic growth after developmental exposure to polychlorinated biphenyls. *Environ Health Perspect*. 2007;115:556-563.
51. Cooper RA, Richter FR, Bays PM, Plaisted-Grant KC, Baron-Cohen S, Simons JS. Reduced hippocampal functional connectivity during episodic memory retrieval in autism. *Cereb Cortex*. 2017;27:888-902.
52. Coskun MA, Loveland KA, Pearson DA, Papanicolaou AC, Sheth BR. Functional assays of local connectivity in the somatosensory cortex of individuals with autism. *Autism Res*. 2013;6:190-200.
53. Khan S, Michmizos K, Tommerdahl M, et al. Somatosensory cortex functional connectivity abnormalities in autism show opposite trends, depending on direction and spatial scale. *Brain*. 2015;138:1394-1409.
54. Aylward EH, Minshew NJ, Goldstein G, et al. MRI volumes of amygdala and hippocampus in non-mentally retarded autistic adolescents and adults. *Neurology*. 1999;53:2145-2150.
55. Barnea-Goraly N, Frazier TW, Piacenza L, et al. A preliminary longitudinal volumetric MRI study of amygdala and hippocampal volumes in autism. *Prog Neuropsychopharmacol Biol Psychiatry*. 2014;48:124-128.
56. Schumann CM, Hamstra J, Goodlin-Jones BL, et al. The amygdala is enlarged in children but not adolescents with autism; the hippocampus is enlarged at all ages. *J Neurosci*. 2004;24:6392-6401.
57. Raymond GV, Bauman ML, Kemper TL. Hippocampus in autism: a Golgi analysis. *Acta Neuropathol*. 1996;91:117-119.
58. Codagnone MG, Podesta MF, Uccelli NA, Reines A. Differential local connectivity and Neuroinflammation profiles in the medial prefrontal cortex and hippocampus in the Valproic acid rat model of autism. *Dev Neurosci*. 2015;37:215-231.
59. Keysers C, Kaas JH, Gazzola V. Somatosensation in social perception. *Nat Rev Neurosci*. 2010;11:417-428.
60. Tavares RM, Mendelsohn A, Grossman Y, et al. A map for social navigation in the human brain. *Neuron*. 2015;87:231-243.
61. Crider A, Nelson T, Davis T, et al. Estrogen receptor beta agonist attenuates endoplasmic reticulum stress-induced changes in social behavior and brain connectivity in mice. *Mol Neurobiol*. 2018;55:7606-7618.
62. Felix-Ortiz AC, Tye KM. Amygdala inputs to the ventral hippocampus bidirectionally modulate social behavior. *J Neurosci*. 2014;34:586-595.
63. Kwon CH, Luikart BW, Powell CM, et al. Pten regulates neuronal arborization and social interaction in mice. *Neuron*. 2006;50:377-388.
64. Brodkin ES, Hagemann A, Nemetski SM, Silver LM. Social approach-avoidance behavior of inbred mouse strains towards DBA/2 mice. *Brain Res*. 2004;1002:151-157.
65. Davis JK, Broadie K. Multifarious functions of the fragile X mental retardation protein. *Trends Genet*. 2017;33:703-714.
66. Tessier CR, Broadie K. The fragile X mental retardation protein developmentally regulates the strength and fidelity of calcium signaling in drosophila mushroom body neurons. *Neurobiol Dis*. 2011;41: 147-159.
67. Rovozzo R, Korza G, Baker MW, et al. CGG repeats in the 5'UTR of FMR1 RNA regulate translation of other RNAs localized in the same RNA granules. *PLoS One*. 2016;11:e0168204.
68. Goncalves JT, Anstey JE, Golshani P, Portera-Cailliau C. Circuit level defects in the developing neocortex of Fragile X mice. *Nat Neurosci*. 2013;16:903-909.
69. O'Donnell C, Goncalves JT, Portera-Cailliau C, Sejnowski TJ. Beyond excitation/inhibition imbalance in multidimensional models of neural circuit changes in brain disorders. *Elife*. 2017;6:e26724. doi: 10.7554/eLife.26724.
70. Qin M, Entezam A, Usdin K, et al. A mouse model of the fragile X premutation: effects on behavior, dendrite morphology, and regional rates of cerebral protein synthesis. *Neurobiol Dis*. 2011;42: 85-98.
71. Lee SH, Park KH, Ho WK, Lee SH. Postnatal developmental changes in Ca2+ homeostasis in supraoptic magnocellular neurons. *Cell Calcium*. 2007;41:441-450.
72. Heng JE, Zurakowski D, Vorwerk CK, Grosskreutz CL, Dreyer EB. Cation channel control of neurite morphology. *Brain Res Dev Brain Res*. 1999;113:67-73.
73. Lacampagne A, Liu X, Reiken S, et al. Post-translational remodeling of ryanodine receptor induces calcium leak leading to Alzheimer's disease-like pathologies and cognitive deficits. *Acta Neuropathol*. 2017;134:749-767.
74. Wayman GA, Bose DD, Yang D, et al. PCB-95 modulates the calcium-dependent signaling pathway responsible for activity-dependent dendritic growth. *Environ Health Perspect*. 2012a;120:1003-1009.
75. Yang D, Kania-Korwel I, Ghogha A, et al. PCB 136 atropselectively alters morphometric and functional parameters of neuronal connectivity in cultured rat hippocampal neurons via ryanodine receptor-dependent mechanisms. *Toxicol Sci*. 2014;138:379-392.
76. Farrell MR, Holland FH, Shansky RM, Brenhouse HC. Sex-specific effects of early life stress on social interaction and prefrontal cortex dendritic morphology in young rats. *Behav Brain Res*. 2016;310: 119-125.
77. Hutsler JJ ZH. Increased dendritic spine densities on cortical projection neurons in autism spectrum disorders. *Brain Res*. 2010;1309: 83-94.
78. Irwin SA PB, Idupulapati M, Jb H, et al. Abnormal dendritic spine characteristics in the temporal and visual cortices of patients with fragile-X

syndrome: a quantitiative examination. *Am J Med Genet*. 2001;98: 161-167.
79. Schmunk G, Gargus JJ. Channelopathy pathogenesis in autism spectrum disorders. *Front Genet*. 2013;4:222.
80. Abrahams BS, Geschwind DH. Advances in autism genetics: on the threshold of a new neurobiology. *Nat Rev Genet*. 2008;9:341-355.
81. Soueid J, Kourtian S, Makhoul NJ, et al. RYR2, PTDSS1 and AREG genes are implicated in a Lebanese population-based study of copy number variation in autism. *Sci Rep*. 2016;6:19088.

SUPPORTING INFORMATION

Additional supporting information may be found online in the Supporting Information section at the end of the article.

How to cite this article: Keil KP, Sethi S, Wilson MD, Silverman JL, Pessah IN, Lein PJ. Genetic mutations in Ca^{2+} signaling alter dendrite morphology and social approach in juvenile mice. *Genes, Brain and Behavior*. 2018;e12526. https://doi.org/10.1111/gbb.12526